Effects of surface roughness on thermo-mechanical fatigue life of a P91 power plant steel

KYAW, Si <http://orcid.org/0000-0001-8568-500X>, ROUSE, J P, LU, J and SUN, W

Available online at www.sciencedirect.com

ScienceDirect

Procedia Structural Integrity 2 (2016) 664–672

Structural Integrity Procedia

www.elsevier.com/locate/procedia

21st European Conference on Fracture, ECF21, 20-24 June 2016, Catania, Italy

Effects of surface roughness on thermo-mechanical fatigue life of a P91 power plant steel

S T Kyaw*[1], J P Rouse[1], J Lu[2], W Sun[1]

1Department of Mechanical, Materials and Manufacturing Engineering, University of Nottingham, Nottingham, Nottinghamshire, NG7 2RD, UK

2Department of Mechanical, Materials and Manufacturing Engineering, University of Nottingham, Ningbo, Zhejiang, China, 315100

Abstract

P91 martensitic steel has now been widely used for power plant components such as steam pipe sections and headers. With the shift to renewable sources, traditional fossil power plants are increasingly expected to operate under so called “two shifting” conditions (high frequency start up/shut down cycles from a partial load condition) to match market demands. Such conditions increase the potential for large thermal stresses to be induced in thick walled components, making thermo-mechanical fatigue (TMF) and creep-fatigue interaction a life limiting concern. It is important to investigate the behaviour of P91 power plant steel under cyclic creep-fatigue interaction conditions in order to estimate the component remnant life under various possible operating strategies. Specimens used for TMF testing are commonly hollow (unlike solid specimens used in isothermal tests) to allow for higher cooling rates (with insignificant radial temperature variations) by injecting air. It is difficult to polish the internal surface to the same extent as the external surface of the specimen (with a roughness (Ra) of 0.8μm). Concerns have been expressed as to whether this type of uncontrolled surface roughness could significantly affect the fatigue life of the specimen since most fatigue cracks often initiate at the surface of the material. In this work, the roughness profile of the internal surface of the TMF sample is measured using Alicona optical profilometer. Resultant surface profiles are idealised and used to simulate distributions of stress and plastic strain under fatigue load using multi-axial visco-plasticity model. Concentration of stress and higher plastic stain accumulations are observed at the peak region of the roughness profile and crack initiations are expected to occur at those regions. Using accumulated plastic strain as a failure criterion for the fatigue, shorter fatigue lifetime is expected for specimen with rougher surface relative to the polished specimen. Optical and scanning electron microscopy (SEM) has been used to investigate the nature of the cracks initiating from the internal and external (polished) surfaces of a failed TMF test specimen.

Peer-review under responsibility of the Scientific Committee of ECF21.

Keywords: P91 steel, surface roughness, visco-plasticity model, thermo-mechanical fatigue

1. Introduction

There is a trend in numerous industries to operate components in ways that ensure output is closely matched to demand. The reasoning for this is clear; by operating based on demand waste can be minimised and efficiency

Peer review under responsibility of the Scientific Committee of ECF21.
10.1016/j.prostr.2016.06.086

increased. A potential danger in this strategy however is that components operating under these conditions will necessarily experience rapidly fluctuating loads that may be both thermal and mechanical. Consequently, ensuring structural integrity against thermo-mechanical fatigue (TMF) is an important priority.

An example of this phenomenon lies in the power industry. The changing energy portfolio has resulted in an increased dependence on renewable energy sources for base load. Conventional thermal plant is therefore becoming required to pick up the deficit to maintain baseline frequency. Given the fluctuations in market demand and renewable energy generation, "two-shifting" operating procedures are increasingly popular (high frequency start up/partial load/shut down cycles) ((Beatt et al., 1983, Shibli and Ford, 2014)). Under such conditions, large thermal stresses can be induced in thick walled high pressure components (such as steam header). In summary, there is a shift in concern in many industries; from creep deformation observed during sustained operation to complex temperature dependent visco-plastic behaviour.

Experimental data is required to determine bulk material properties in order to characterise these behaviours at the continuum level. For cyclic loading conditions, visco-plastic deformation and damage may be approximated using, for example, the material models presented in (Chaboche and Rousselier, 1983a, Chaboche and Rousselier, 1983b, Lemaitre and Chaboche, 1994). While solid specimens can be used for isothermal testing, it is generally the case that hollow samples are used for scenarios where both mechanical and thermal loads fluctuate (such as during TMF). Very high heating rates can be achieved in the laboratory using induction heating or radiant lamps. To match these rates (and achieve regular loading waveforms that may be analysed) when cooling is required, forced air is typically injected through the specimen. External surfaces of the specimen may be easily polished to $R_a = 0.8\mu m$, meaning machining defects (that would cause highly localised stress concentration) can be removed. Internal surfaces that are drilled in hollow samples cannot be controlled so easily. A concern exists therefore in the validity of TMF experiments performed using hollow samples. The work of Whittaker et al. (2013) for instance demonstrates the initiation of cracks on the internal surface of a hollow nickel based superalloy specimen tested to failure under TMF loading conditions. If localised behaviour in the vicinity of machining marks is severe premature crack imitation may be observed and bulk gauge section results distorted. These concerns are intensified when the work of Murakami and Miller (2005) is considered. Their investigations into fatigue damage in 70/30 brass highlighted that, rather than the approach assumed by continuum damage mechanics (CDM) by designating a representative volume element (RVE), the loss in load carrying capability during fatigue loading was dominated by crack initiation at the surface only. If surface conditions on a specimen are poorly understood, it is foreseeable that "fatigue damage" will be over-estimated or misinterpreted. The present work looks to investigate the possible effect of machining surface features on localised cyclic visco-plastic behaviour by conducting a stochastic study of drilled (internal) and polished (external) samples, reconstructing representative unit cells and subjecting them to cyclic loading in finite element analysis (FEA) using a multi-axial viscoplasticity model. The lifetime for fatigue crack initiation was also estimated using accumulated plastic strain and stored energy approach.

2. Surface analysis

To achieve faster cooling and heating rates, TMF samples used by Saad (2012) have a 4mm diameter through hole and its geometry and dimensions are shown in Fig. 1. The internal surface of a hollow sample is complex with features being semi-periodic and several different orders of "roughness" superimposed. Simulation of individual features observed from micrograph would be of limited interest as the severity of the feature could not be compared to others in the sample. What follows in the present section therefore is a description of the stochastic approach employed to generate representative unit cells based on observed surface profiles.

3D surface maps have been determined for "polished" (representative of the external $R_a = 0.8\mu m$ surface of a test specimen) and "drilled" (representative of the machined internal surface) test coupons using an Alicona Infinite Focus (http://www.alicona.com/en/products/infinitefocus, 2016.). Surfaces were imaged using a 10x objective lens, suggesting a vertical (z axis) resolution of 150nm. This is deemed to be appropriate given the scale of features expected on the external polished (control) surface. The 4mm diameter hole machined in the "drilled" test coupon was cut using a tool spindle speed of 600rpm and a feed rate of 0.1mm/rev. Standard white water soluble oil coolants were used during the process. These parameters are typical of machining processes performed on high strength steels such as P91. The post-processing of the measured roughness profiles were carried out using MATLAB.

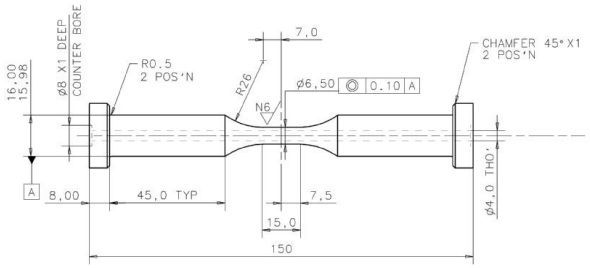

Fig. 1: Geometry and dimensions of a TMF specimen used by Saad (2012)

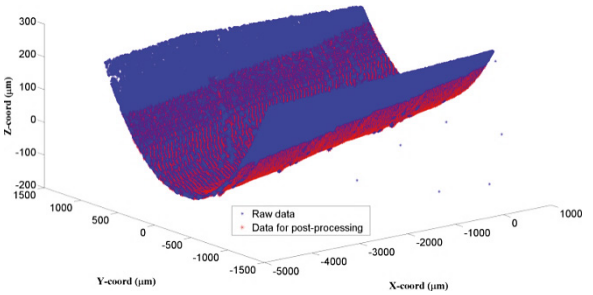

Fig. 2: Raw roughness points measured by Alicona; a region used for post-processing is highlighted in red

A raw surface profile measured by Alicona is plotted in Fig. 2. The data for surface heights are stored as Z coordinates as a function of X and Y coordinates. There are some visible noise data within this sample especially near the edge of the cylinder where the edges are sharp. The actual area for post processing purposes is highlighted in red as shown in Fig. 2. Randomly selected 2D surface profiles in X-Z coordinate system are illustrated in Fig. 3. Each profile is taken along the line of a fixed Y coordinate (parallel to the axis of the test specimen/drilled hole). From those profiles, a linear trend can be seen and it corresponds to the "form" of the test coupon (its general shape and size). After removing a linear trend from the data, the roughness profiles are illustrated in Fig. 4. From these data, both "waviness" (low frequency variations) and "roughness" (high frequency variations) profiles with two different scales of wavelength can be observed. Moreover, unrealistically high peak points can also be found and these points could be either signal noise or are given by dust collected on the sample. To extract a periodic roughness profile that can be used for FEA, Fourier transforms are taken to convert the continuous spatial data in the specific domain to the frequency domain. It is based on the concept that any complex and continuous data can be represented by combinations of sinusoids and each sinusoid can be characterised by its amplitude and frequency. In this case, Z-coords in X domain are transformed into frequency domain. A statistical distribution study for each fundamental frequency is carried out here to obtain a representative unit cell to represent the idealised roughness profile and to be used for finite element analysis (FEA).

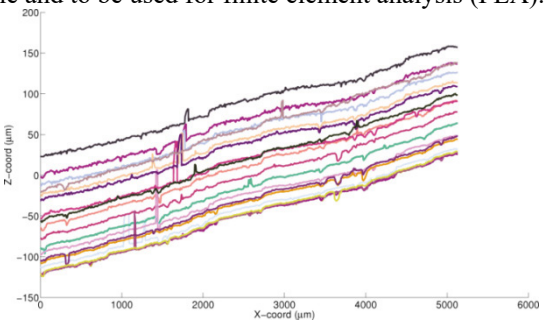

Fig. 3: Random 2D surface profiles in X-Z coordinate system

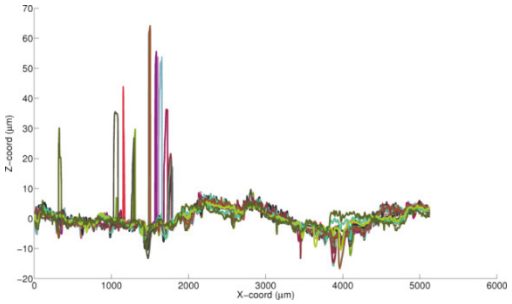

Fig. 4: Random 2D surface profiles in X-Z coordinate system after linear detrending

To carry out a distribution study, random 2D surface profiles have to be chosen from available data. In this study 200 surface profiles were randomly chosen. Each surface profile has X domain length of approximately 5000µm. From each surface profile, a sample of 300µm is extracted. An example Fourier transform distribution of one of the roughness profiles used for distribution study is illustrated in Fig. 5. After transforming 200 roughness profiles, the distribution study on amplitudes, phase shifts and frequencies of first 15 fundamental waves are carried out and representative roughness is reconstructed using mean and one standard deviation of amplitudes and frequencies. This process was repeated for five times resulting in the profiles shown in Fig. 6. The amplitudes of the asperities vary from 3-10µm and the periodicities vary from 60-200µm. Two different types of unit cells; one with a full sinusoidal wave and the other with half sinusoidal waves were chosen for FEA as shown in Fig. 7. Three sets of A and L taken for the analysis are 9µm and 60µm, 6µm and 80µm and 9µm and 200µm, respectively.

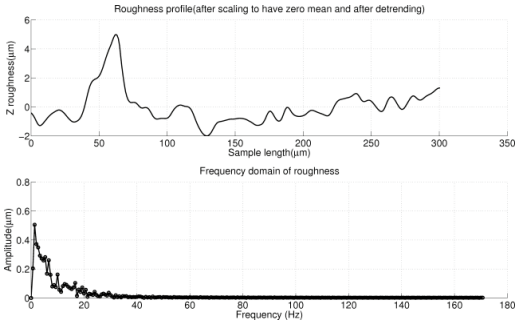

Fig. 5: A fourier transform of one of the roughness profiles

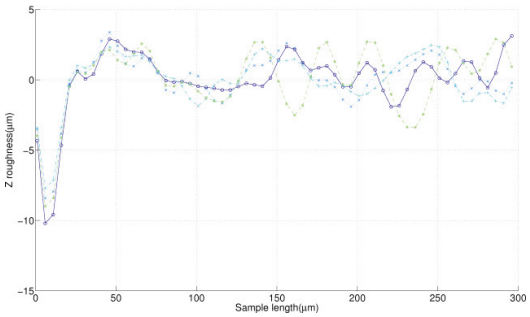

Fig. 6: Representative surface roughness given by five different distribution studies of roughness data

3. Finite element analysis (FEA) of a hollow TMF specimen

The geometry and boundary conditions used in the FEA simulations are shown in Fig. 7. The model represents a hollow cylinder (the TMF sample used in (Saad, 2012)) with an assumed smooth outer surface (representative of the polished R_a = 0.8μm surface). On the other hand, two different types of surface roughness profile (sinusoid and half-sinusoid) with three sets of aspect ratios determined from the Fourier analysis were used to represent the idealised internal surface. The profiles are assumed to be periodic along the axial axis of the cylinder.

The loading used for the simulation is a strain controlled low cycle fatigue loading profile (strain range of ±0.5% with strain rate of 0.033 %/s). The loading profile is a fully reversed with a zero mean. The temperature profile is in-phase (IP) with the applied load and it varies between 400˚C-500˚C with the rate of 3.33˚C /s. The period of the cycle is 60s and total cycle is 600. This loading is identical to the loading for one of the experiments by Saad (2012). Although a uniaxial loading is applied, the stress state is expected to be multiaxial around the roughness feature. For comparison purpose, a single element model which represents the uniaxial loading case without a roughness feature was also modelled.

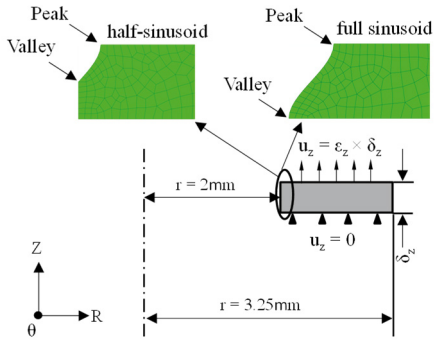

Fig. 7: Geometry and boundary conditions of unit cell used for FEA, and FE meshes of roughness profiles used for the internal surface of the unit cell

4. Viscoplastic material model

When TMF loading is applied to P91 steel at high temperatures the material exhibits viscoplastic behaviour (Bernhart et al., 1999, Zhang et al., 2002, Saad et al., 2011). In the multiaxial form, the relationship between viscoplastic strain rate ($\dot{\varepsilon}_{ij}^{p}$) and stress can be expressed by power law relationship:

$$\dot{\varepsilon}_{ij}^{p} = \frac{3}{2}\left(\frac{f}{Z}\right)^{1/n} \frac{\sigma_{ij}^{'} - \chi_{ij}}{J\left(\sigma_{ij}^{'} - \chi_{ij}\right)} \tag{1}$$

where Z and n are material parameters. f is known as a yield function and determines the elastic limit; the material yields when f is greater than zero (see Eq (2), where $J\left(\sigma_{ij}^{'} - \chi_{ij}\right)$ is defined by Eq (3) and is the second invariant of the stress tensor). A von Mises yield criterion is assumed for the P91 material.

$$f = J\left(\sigma_{ij}^{'} - \chi_{ij}\right) - R - k \tag{2}$$

$$J\left(\sigma_{ij}^{'}-\chi_{ij}\right)=\left(\frac{3}{2}\left(\sigma_{ij}^{'}-\chi_{ij}^{'}\right):\left(\sigma_{ij}^{'}-\chi_{ij}^{'}\right)\right)^{1/2} \tag{3}$$

Eq (2) shows the yielding point depends on kinematic hardening (χ), isotropic hardening (R) parameters which evolve due to inelastic loading. The present state of the material therefore depends on its loading history through these quantities and the constant cyclic yield strength (k) (the initial size of the yield locus). χ and R also known as back stress and drag stress, respectively, and can be expressed in terms of effective plastic strain (accumulated over loading cycles) under anisothermal conditions (Zhang et al., 2002) using Eq (4) and (5) respectively.

$$\dot{R}=b(Q-R)\dot{p}+H\dot{p}+\left(p\frac{\partial H}{\partial T}+\left((R-Hp)\left(\frac{1}{Q}\frac{\partial Q}{dT}+\frac{1}{b}\frac{\partial b}{dT}\right)\right)\right)\dot{T} \tag{4}$$

$$\dot{\chi}_{ij}=\sum_{z=1}^{2}\frac{2}{3}C(z)\left(a(z)\dot{\varepsilon}_{ij}^{p}-\chi_{ij}\dot{p}\right)+\left(\frac{1}{C(z)}\frac{\partial C(z)}{\partial T}+\frac{1}{a(z)}\frac{\partial a(z)}{\partial T}\right)\chi_{ij}\dot{T} \tag{5}$$

Q, b, H are material constants relating to the drag stress. C and a are material constants relating to back stress and two sets of C and a are used to describe nonlinear behaviour of the material. Under multiaxial loading, rate of plastic strain $\left(\dot{\varepsilon}_{ij}^{p}\right)$ is related to the rate of effective plastic strain ($\dot{p}$) by Eq (6).

$$\dot{\varepsilon}_{ij}^{p}=\dot{p}*n_{ij} \tag{6}$$

n_{ij} is the normal vector to the tangent to the yield surface at the load point and it can be shown to have the following identity:

$$n_{ij}=\frac{\partial f}{\partial\sigma_{ij}}=\frac{3}{2}\frac{\sigma_{ij}^{'}-\chi_{ij}}{J\left(\sigma_{ij}^{'}-\chi_{ij}\right)} \tag{7}$$

where $\sigma_{ij}^{'}$ is the deviatoric stress tensor and σ_{eq} is the von Mises equivalent stress. Using Eq (2) and Eq (7) the viscoplastic law can be expressed in terms of the effective stress and effective plastic strain as shown in Eq (8). A material subroutine (UMAT in Abaqus) has been written to solve Eq (1) to Eq (8) simultaneously for viscoplastic behaviour of P91 steel.

$$\dot{p}=\left(\frac{f}{Z}\right)^{1/m} \tag{8}$$

At the beginning of a time step a thermal strain (the product of coefficient of thermal expansion (CTE) and temperature difference) is subtracted from the total strain to determine the corresponding mechanical strain for the plasticity routine. CTE values for P91 are taken from ThyssenKrupp Materials International (2011). A semi-implicit scheme (Dunne and Petrinic, 2005) is used for updating plastic strain within the UMAT. The dependence of drag and back stresses on the temperature rate are updated at the beginning of each time step using the total accumulated plastic strain (p) from the previous time step (assuming that increments to p are small).

The material properties of P91 (8.6Cr 1.02Mo 0.12C 0.34Si 0.24V 0.017P 0.07Nb 0.06N 0.03W wt%) for the above viscoplastic model are temperature dependent. They are determined from uniaxial fatigue test data collected by Saad (2012) under isothermal conditions. For each temperature case, the aforementioned viscoplastic model is used in conjunction with the optimisation procedure outlined in (Gong et al., 2010) to obtain representative material constants. A summary of material constants assumed for P91 at 400˚C and 500˚C are tabulated in

Table 1.

Table 1: Material parameters for viscoplastic model for P91 steel.

Temp (˚C)	a_1 (MPa)	C_1	a_2 (MPa)	C_2	Z (MPa•s$^{1/n}$)	n	b	-Q (MPa)	k (MPa)	E (MPa)	-h
400	131.036	504.897	49.8521	1999.998	2400	1.789	0.7	35	225	167595.9	1.8
500	95	521.9532	29.23425	1140.859	3000	1.9	1.1	43	210	160182.7	2.35

5. Results and discussions

Stress-strain hysteresis loops obtained from a single element (uniaxial) model loaded under TMF conditions

(fully reversed in phase 400°C-500°C, ±0.5%, with a cycle time of 60s) at 1st and 200th cycles, and at 300th and 500th cycles are shown in Fig. 8 and Fig. 9, respectively. A good level of agreement may be observed between experimental and simulated stresses (determined from the UMAT). Accurate predictions of maximum and minimum stresses (<1% error) are evident. High errors (50MPa) are noted however in the hardening region itself. This suggests that although the saturated value for kinematic hardening stress can be predicted accurately from the isothermal results, further work is required to predict the rate of saturation (which determines the hardening stress profile).

If the specimen surface is perfectly smooth, the stress of the test specimen is (of course) uniform under uniaxial TMF load and a single cell model can be used to simulate the test. However, localised multiaxial stress states are expected in the vicinity of the roughness features. von Mises stress distributions for two different types of roughness profiles at the end of 600 cycles of loading are shown in Fig. 10. The stresses in the valley region of the sinusoid model are about twice as high as the stresses at the valley of the half-sinusoid model. Nevertheless, significant premature yielding is expected at the peak region for both models due to the large stress concentration effects. Stress states are still predominantly uniaxial (stresses in the loading direction (σ_{22}) are more than 600 times higher than stresses in the other directions) for the area some distance away (> 0.1mm) from the roughness features. The stresses at these regions are close to those predicted by a single element model. The ratios of maximum and minimum values of stresses (σ_{22} and σ_{Mises}) at the peak and valley of the sinusoid (A6L80) to the uniaxial stress given by a single element model are plotted in Fig. 11 to highlight the significant increase in stresses at the peak region.

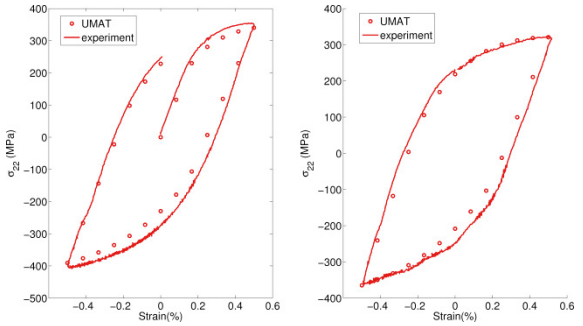

Fig. 8: Comparisons of stress (σ_{22}) of a single cell model to experimental results (Saad, 2012) at (i) 1st and (ii) at 200th cycle

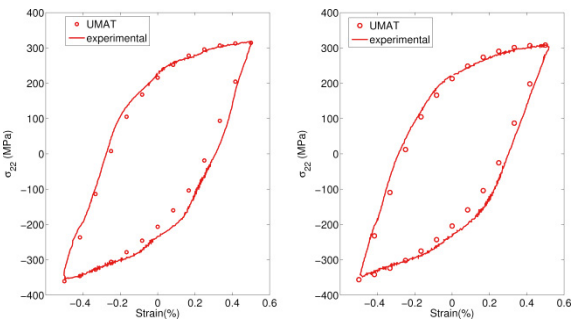

Fig. 9: Comparisons of stress (σ_{22}) of a single cell model to experimental results (Saad, 2012) at (i) 300th and (ii) at 500th cycle

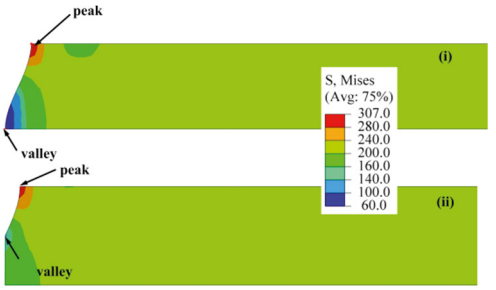

Fig. 10: σ_{22} stress contours of (i) sinusoid and (ii) half-sinusoid unit cells (A = 6μm and L = 80 μm) at the end of 600 cycles of loading.

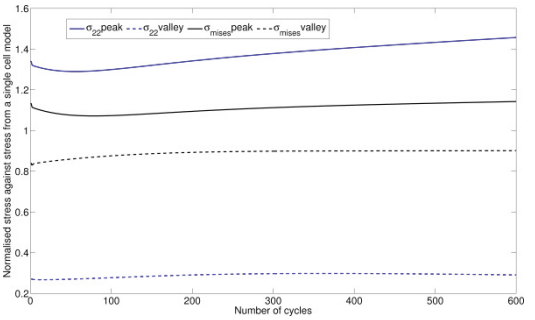

Fig. 11: Evolutions of stress in the loading direction (σ_{22}) and σ_{Mises} at the peak and valley of the sinusoid (A6L80) normalised with σ_{22} from the a single cell model

When P91 is subjected to TMF loading, the cyclic softening of the material (reduction in maximum stress of a cycle) is expected after each cycle, caused by isotropic softening (Saad, 2012). The drag stress (R, which represents isotropic effects) is directly proportional to p as shown in Eq (4). Since yielding and plastic strain occur when the von Mises stresses are higher than the yield strength, areas with higher stress concentration are also expected to have higher magnitude of p and hence, R. R at the peak and the valley of the sinusoid model (A6L80) and R from the uniaxial model are compared in Fig. 12. Due to very low p, R has not reached the stabilised value (~60MPa) at the

valley. Both R at the peak and from the uniaxial model stabilises around p=3% and subsequent softening is from a linear isotropic term.

Researchers (Giroux, 2011, Chaboche, 1996, Chaboche, 2008, Lemaitre and Chaboche, 1994) have linked the energy stored from cyclic softening (area under the curves of Fig. 12) to the initiation of cracks from creep-fatigue damage. For the uniaxial model, the energy stored after 600 cycles is expected to be around 213 MJ/m^3 whereas for the peak of the sinusoid model (A6L80), it is 898 MJ/m^3. Higher aspect ratio also gives higher increase in p per cycle as shown in Fig. 13 whereas uniaxial case gives the lowest p. Since the stabilised R value is expected to be similar for all cases for identical loading and material, this means that energy stored will be higher for higher aspect ratios (due to increased accumulation rates for p).

To estimate the energy for crack initiation, isothermal fatigue tests at 600˚C with polished surfaces were used (Saad, 2012). The energy for crack initiation varies between 830-1000 MJ/m^3 and it is assumed that the stored energy for crack initiation is independent of loading condition. Hence cracks are expected to initiate at the peak region of the sinusoid before ultimate failure. This also indicates that using uniaxial model will under-predict the energy stored and crack initiation time. Therefore, use of multiaxial model (with roughness features) is required to predict the initiation of local cracks. The propagation of these local cracks at roughness features could eventually lead to loss of stiffness and a drop in the load carrying capacity of the material. These observations are similar to those made by Murakami and Miller (2005), where it was shown that ductility can be restored in an apparently "damaged" sample by removing the surface layer of material (demonstrating that fatigue damage development could be controlled by micro-crack initiation and propagation at the surface of a material only).

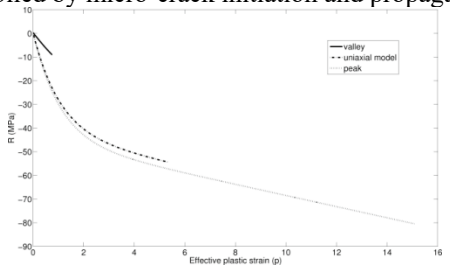

Fig. 12: Drag stress evolution against accumulated plastic strain of peak and valley at internal roughness features (A6L80) and of a uniaxial model

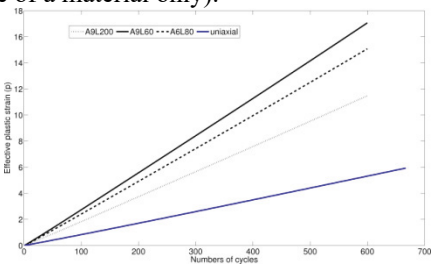

Fig. 13: Effective plastic strain accumulation at the peak of the sinusoid with different aspect ratios and for uniaxial model

To observe possible crack initiation sites, optical micrographs of sections of one of the failed TMF specimens from Saad (2012) were taken. The history of loading for the specimen is identical to the one used in this paper (400-500˚C in-phase (IP) fatigue loading with strain range of ±0.5%). Fig. 14 shows different locations of both internal and external sides of the specimen. In contrary to CDM damage theory (Chaboche, 2008, Lemaitre and Chaboche, 1994), no voids (characteristic of classical creep damage) are visible across the specimen. On the other hand, several surface cracks can be observed at both internal and external surfaces. Moreover, SEM images of specific internal cracks indicate that the cracks are found in the vicinity of the peak of the roughness asperities. This finding supports the predicted results obtained from FEA that suggest roughness features are predominant crack initiation sites.

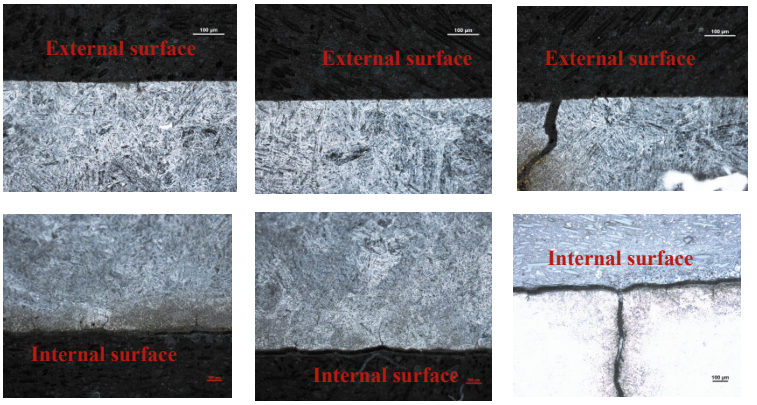

(i)

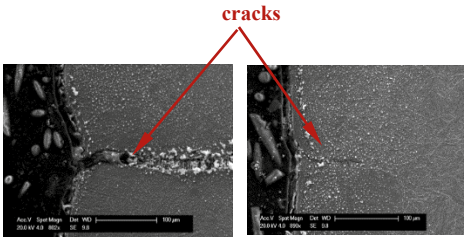

(ii)

Fig. 14: (i) Optical images of cracks along the internal and external surfaces of the TMF specimen subjected to 400-500˚C IP load and (ii) SEM image of the internal cracks near the peak of the roughness asperity

6. Conclusions

In this work, the effect of surface roughness of a hollow TMF specimen on crack initiation and lifetime under fatigue load was studied. The surface roughness due to a drilling process on a test coupon was measured using an optical profilometer. Using these results several characteristic unit cells (roughness profiles) were created and analysed using FEA. Multiaxial FEA was carried out using a viscoplastic material model. The results indicate that the energy stored at the peak of a roughness feature (after 600 TMF cycles) could be almost 4 times that observed in the typical uniaxial (smooth) model and is more in keeping with the energy levels expected for crack initiation. This demonstrates the inadequacy of using the uniaxial model for prediction of TMF life even if the tests are carried out under (apparent) uniaxial load conditions. Due to the direct proportional relationship between plastic strain accumulation and aspect ratio features with higher aspect ratios could accelerate the initiation of surface cracks. Optical images of failed TMF specimens show no voids within the specimen but multiple initiated surface cracks. Hence, damage initiation and accumulation models assumed in classical CDM might not be suitable for P91 under fatigue loading and alternative initiation criterion based on surface features may be required. Further investigations are required however to examine the specimen subjected to temperatures greater than 500˚C. SEM images of internal cracks at the peaks of roughness features reaffirm the predicted crack initiation sites (from FEA). These surface cracks can drive the loss of stiffness of the specimen (often misidentified as bulk damage), leading to failure. Methodologies presented in this paper can be applied to numerous engineering structures that experience TMF loading conditions to predict crack initiation sites by locating the local areas with large accumulated plastic strains.

Acknowledgement

We would like to acknowledge the support of the Engineering and Physical Sciences Research Council (EPSRC) for their support for the project - Flexible and Efficient Power Plant: Flex-E-Plant (Grant number: EP/K021095/1). We also thank the following partners for their valuable contributions: Alstom Power Limited, Doosan Babcock Limited, Centrica plc., EDF Energy (West Burton Power) Limited., E.ON Technologies (Ratcliffe) Limited, Goodwin Steel Castings Limited, NPL Management Limited, R-MC Power Recovery Limited., RWE Generation UK plc., Scottish and Southern Energy (SSE) plc., Siemens Industrial Turbomachinery and TWI Limited. The authors would like to thank Adam Thompson and Dr. Su Rong of the Manufacturing Metrology Team for their contributions in surface roughness measurements using focus variation microscopy.

References

Beatt, R. J. I., Birch, W. L., Hinton, S. E., Kelly, M., Pully, M.J., 1983. Two-Shift Operation of 500 MW Boiler/Turbine Generating Units. . Proceedings of the Institution of Mechanical Engineers, Part A: Journal of Power and Energy, 197**,** 247-255.

Bernhart, G., Moulinier, G., Brucelle, O., Delagnes, D. 1999. High temperature low cycle fatigue behaviour of a martensitic forging tool steel. International Journal of Fatigue, 21**,** 179-186.

Chaboche, J. L. 1996. Unified cyclic viscoplastic constitutive equations. Development, capabilities and thermodynamic framework. In: Krausz AS, Krausz K, editors. Unified constitutive laws of plastic deformation. San Diego, USA: Academic Press.

Chaboche, J. L. 2008. A review of some plasticity and viscoplasticity constitutive theories. International Journal of Plasticity, 24**,** 1642-1693.

Chaboche, J. L., Rousselier, G. 1983a. On the Plastic and Viscoplastic Constitutive Equations—Part I: Rules Developed With Internal Variable Concept. Journal of Pressure Vessel Technology, 105**,** 153-158.

Chaboche, J. L., Rousselier, G. 1983b. On the Plastic and Viscoplastic Constitutive Equations—Part II: Application of Internal Variable Concepts to the 316 Stainless Steel. Journal of Pressure Vessel Technology, 105**,** 159-164.

Dunne, F., Petrinic, N. 2005. Introduction to Computational Plasticity. Oxford University Press.

Giroux, P.-F. 2011. Experimental study and simulation of cyclic softening of tempered martensite ferritic steels.PhD thesis. Ecole Nationale Superieure des Mines de Paris.

Gong, Y. P., Hyde, C. J., Sun, W., Hyde, T. H. 2010. Determination of material properties in the chaboche unified viscoplasticity model. Proceedings of the Institution of Mechanical Engineers, Part L: Journal of Materials: Design and Applications, 224**,** 19-29.

http://www.alicona.com/en/products/infinitefocus 2016.

Lemaitre, J., Chaboche, J. L. 1994. Mechanics of Solid Materials. Cambridge University Press, .

Murakami, Y., Miller, K. 2005. What is Fatigue Damage? A View Point from the Observation of Low Cycle Fatigue Process. International Journal of Fatigue, 27**,** 991-1005.

Saad, A. A. 2012. Cyclic plasticity and creep of power plant materials. PhD thesis. University of Nottingham.

Saad, A. A., SUN, W., HYDE, T. H., TANNER, D. W. J. 2011. Cyclic softening behaviour of a P91 steel under low cycle fatigue at high

temperature. Procedia Engineering, 10**,** 1103-1108.
Shibli, J. L., Ford, J. 2014. Damage to Coal Power Plants due to Cyclic Operation. In:Shibli A, editor. Coal Power Plant Materials and Life Assessment: Developments and Applications.Woodhead Publishing p. 333-357.
Thyssenkrupp Materials International 2011.
http://www.s-k- h.com/media/de/Service/Werkstoffblaetter_englisch/Kesselrohre_ASTM/P91_T91_engl.pdf.
Whittaker, M., Lancaster, R., Harrison, W., Pretty, C., Williams, S. 2013. An Empirical Approach to Correlating Thermo-Mechanical Fatigue Behaviour of a Polycrystalline Ni-Base Superalloy. . Materials, 6**,** 5275-5290.
Zhang, Z., Delagnes, D., Bernhart, G. 2002. Anisothermal cyclic plasticity modelling of martensitic steels. International Journal of Fatigue, 24**,** 635-648.